Advances in Science and Technology Research Journal

Advances in Science and Technology Research Journal, 2026, 20(6), 298–313
https://doi.org/10.12913/22998624/217958
ISSN 2299-8624, License CC-BY 4.0

Received: 2025.11.22
Accepted: 2026.04.15
Published: 2026.05.01

Influence of bar diameter, embedment length, and thermal exposure on the bond strength between ultra-high performance concrete and reinforcing steel

Abduljaleel Al-Janabi[1*], Majid M.A. Kadhim[1]

[1] College of Engineering, Department of Civil Engineering, University of Babylon, Babil, 51002, Iraq
* Corresponding author's e-mail: abduljaleel.al-janabi.engh407@student.uobabylon.edu.iq

ABSTRACT

This study investigates the bond behavior between ultra-high-performance concrete (UHPC) and reinforcing steel subjected to elevated temperatures, with a focus on the influence of embedment length, concrete cover, and thermal exposure. Using the beam-end test method in accordance with Eurocode recommendations, a series of specimens were prepared with varying diameters (12 and 16 mm), embedment lengths (6d, 9d, and 12d (d: bar diameter)), concrete cover depths (1d and 2d), and exposed to three temperature conditions: room temperature (25 °C), 300 °C, and 600 °C. The results demonstrated that temperature has a substantial effect on bond performance. While moderate heating (300 °C) sometimes enhanced bond strength due to post-curing effects, exposure to 600 °C caused significant bond degradation, characterized by reduced load capacity and increased slippage. Longer embedment lengths consistently improved bond strength across all temperatures, often shifting failure modes from pull-out to steel rupture. Increased concrete cover provided better confinement and thermal protection, though its influence was less dominant under severe thermal exposure. The findings contribute to a deeper understanding of the bond mechanisms in UHPC-steel systems and offer practical insights for the structural design of UHPC elements in thermally demanding environments, including fire-prone applications.

Keywords: ultra-high performance concrete, reinforcing steel, bond strength, elevated temperatures.

INTRODUCTION

Concrete, a fundamental construction material, relies on reinforcing steel to compensate for its low tensile strength. However, conventional reinforced concrete faces durability issues, particularly steel corrosion, leading to high maintenance costs and reduced service life [1, 2]. This has driven the development of advanced cementitious composites like high-performance concrete (HPC) and ultra-high-performance concrete (UHPC) [3].

HPC offers superior mechanical strength, durability, and reduced permeability, making it suitable for demanding structures [4, 5]. Its economic benefits stem from reduced material use and faster construction [6–8]. UHPC, a more advanced class, typically exceeds 120 MPa in compressive strength and exhibits unique elastic-plastic characteristics under tension due to its dense microstructure and often high steel fibre content [9]. Key distinctions of UHPC include the absence of coarse aggregates, low water-to-cement ratio, and optimized particle packing, resulting in exceptional strength and durability [10, 11].

The bond between concrete and reinforcing bars is crucial for composite action, transferring forces and ensuring structural integrity [12]. This interaction is facilitated by similar thermal expansion coefficients, minimizing bond loss under temperature fluctuations [13]. With increasing UHPC adoption, understanding its bond behaviour at elevated temperatures is critical. Existing research on UHPC properties is extensive, but a knowledge gap persists regarding its bond performance during and after high-temperature exposure, which is crucial for fire safety and structural integrity.

This research aims to experimentally investigate the bond behavior of UHPC-steel systems under varying elevated temperatures (room temperature 25 °C), 300 °C, and 600 °C. Specific objectives include quantifying the influence of embedment length (6d, 9d, 12d) and concrete cover (1d, 2d) on bond strength and failure modes, analyzing load-slip characteristics, identifying critical temperature thresholds for bond degradation, providing design insights for thermally demanding environments, and developing a predictive model for bond stress.

This study addresses a critical knowledge gap concerning UHPC-steel bond performance under elevated temperatures, vital for structural safety in fire events. Findings will contribute to accurate design guidelines for UHPC applications, particularly in fire-resistant construction. Identifying influential parameters offers practical insights for optimizing reinforcement detailing, enhancing resilience, and extending service life. Ultimately, this research provides essential data for the safe and effective use of UHPC in demanding applications.

The study focuses on the experimental investigation of bond behaviour between deformed reinforcing steel bars (12 mm and 16 mm diameters) and UHPC. Parameters include embedment lengths (6d, 9d, 12d), concrete cover depths (1d, 2d), and elevated temperatures (room temperature, 300 °C, 600 °C). The beam test method, consistent with Eurocode, is used. UHPC mechanical properties (flowability, compressive, tensile strength) are characterized before studying the bond stresses.

The study is limited to specific bar diameters, embedment lengths, concrete cover depths, and three discrete temperature points. It focuses on static loading after thermal exposure, excluding dynamic or cyclic conditions. The influence of different UHPC mix designs is not extensively explored, nor are the effects of various cooling regimes.

BACKGROUND

UHPC is an advanced cementitious composite known for exceptional mechanical properties and durability, achieved through high fine powder content, low water-to-binder ratio, and often steel fibres [10, 11]. UHPC is defined by its ultra-high compressive strength, typically exceeding 120 MPa, allowing for slender structural elements [9]. With steel fibres, it exhibits remarkable tensile performance and strain-hardening behaviour, distinguishing it from brittle conventional concrete [14]. UHPC's thermal properties are crucial for fire-prone applications. Its dense matrix and low permeability influence its behaviour under elevated temperatures. Concrete undergoes physical and chemical changes, including dehydration (above 100 °C), decomposition of C-S-H gel (above 300 °C), and significant strength reduction beyond 600 °C [15–17]. UHPC's density can increase spalling risk due to trapped steam pressure during rapid heating [18, 19].

The bond between concrete and reinforcing steel is a critical mechanism that enables reinforced concrete to function as a composite material. This bond allows for the transfer of forces between the two materials, ensuring their collaborative structural behaviour.

Fundamental bond mechanisms

The bond between concrete and reinforcing steel is a complex phenomenon involving chemical adhesion, friction, and mechanical interlock [20]:

- Chemical adhesion The cement paste adheres to the surface of the reinforcing bars which results from chemical and physical interactions at the interface. However, this bonding strength is relatively weak and can be break under high stresses leading to reliance on other mechanisms [21].
- Frictional resistance Once the chemical adhesion is compromised, frictional forces develop between the steel surface and surrounding concrete. These frictional forces increase when the bar is subjected to compressive stresses perpendicular to its surface, providing resistance against slip [1, 21].
- Deformed bars This is the primary bond mechanism. The ribs or lugs on deformed bars provide mechanical anchorage against the surrounding concrete [14, 22]. When tensile forces are applied to the bar, the ribs bear against the concrete, transferring stresses through mechanical interlock, Figure 1 [6].

Bond failure mechanisms in reinforced concrete

Bond is influenced by bar properties (diameter, surface condition, yield strength), concrete properties (compressive/tensile strength, mix design), and environmental factors (temperature,

moisture content) [31, 33, 35]. Elevated temperatures degrade both concrete and the steel-concrete interface due to dehydration, thermal expansion, and material property changes [25, 26, 31]. Three main bond failure mechanisms occur in reinforced concrete, Figure 2.

- Pull-out failure bar pulls out without significant concrete cracking, common with short embedment or well-confined concrete
- Splitting failure radial stresses exceed concrete tensile strength, causing longitudinal cracks, prevalent with insufficient cover, Figure 2.
- Steel rupture occurs when bond capacity exceeds steel tensile strength, leading to bar yielding and rupture.

Bond between concrete and reinforcing bars under elevated temperatures

Research shows bond strength generally decreases with increasing temperature, influenced by concrete type, bar diameter, embedment, and confinement [23]. Moderate temperatures (up to 300 °C) may not significantly reduce, or even slightly enhance, bond due to post-curing. However, severe degradation occurs beyond 400–600 °C due to cementitious phase decomposition and differential thermal expansion [18, 24].

UHPC's dense microstructure can offer better fire resistance but risks spalling due to trapped moisture [15, 17]. Steel fibres in UHPC can mitigate spalling and improve residual mechanical properties, positively influencing bond after thermal exposure [8]. Studies by Xu et al. [23] and others [25] confirm the benefits of fibres and the need for experimental data on UHPC bond behaviour under thermal loads.

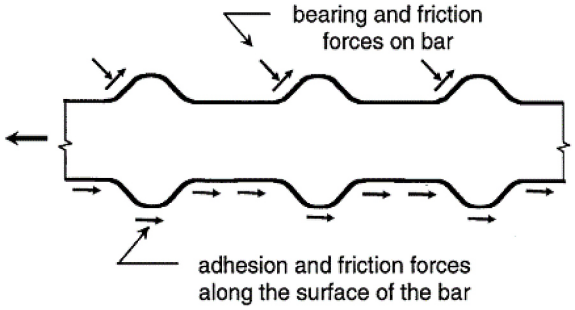

Figure 1. Bond force transfer mechanism [1]

RESEARCH METHODOLOGY

Experimental program

The experimental procedure included the Specimen preparation by making plywood moulds with internal dimensions of (800 × 180 × 100) mm according to RILEM [27]. The beam-bond test procedure used in this study is based on the guidelines outlined in the PN-EN 10080 standard [28]. The test procedure is outlined in full detail below:

The study systematically investigated UHPC–steel bond behaviour under varying temperatures and geometric parameters using the Eurocode-recommended beam test method [27].

Figure 3 give the dimensions of the UHPC specimen used for the bond test. A full detail for the auxiliary reinforcement is illustrated in Figure 5.

Deformed reinforcing steel bars of 12 mm and 16 mm diameters were cleaned and prepared. Embedment lengths were precisely controlled at 6d, 9d, and 12d.

Custom moulds ensured precise specimen dimensions and accurate positioning of bars and concrete cover depths (1d and 2d).

UHPC preparation

Materials used

The UHPC mixture was formulated using locally sourced V-type sulphate-resistant cement, which was laboratory-verified to meet the standards specified by Iraqi construction material regulations. Fine sand from Najaf, characterized by a maximum particle size of 0.6 mm, was also employed in accordance with the same national standards. High-purity quartz powder was procured from Al-Nawafidh Company, based in Najaf. The mix was reinforced with brass-coated steel fibres measuring 13 mm in length and 0.22 mm in diameter, exhibiting a high tensile strength of up to 2860 MPa. Additionally, MasterRoc MS 610 was utilized as a silica fume source, complemented by MasterGlenium 51 as a high-range water-reducing admixture (superplasticizer), and reverse osmosis (RO) water was used for mixing to ensure material purity.

Mixing proportion

A comprehensive series of experimental trials was carried out involving different types of cement, various mix proportions, and alternative

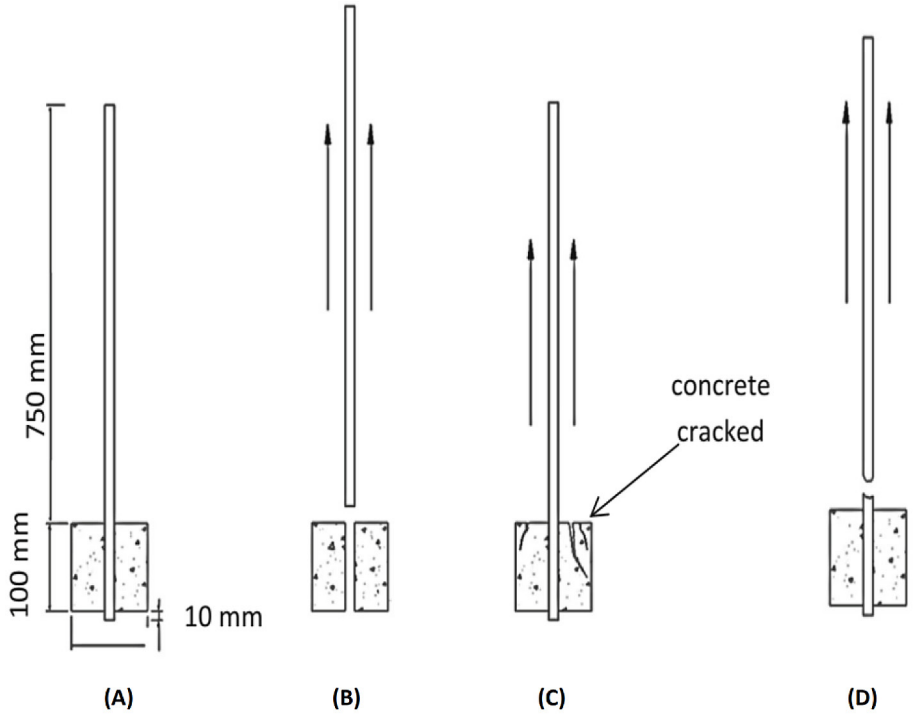

Figure 2. Typical bond failure modes observed in the pull-out test: (A) original specimen, (B) pull-out failure of the reinforcing bar, (C) concrete splitting failure, and (D) rupture of the reinforcing steel [26]

mixing techniques in order to determine the optimal UHPC composition. The finalized mix design, presented in Table 1, outlines the constituent material quantities per cubic meter of UHPC.

Mixing procedure

The UHPC mixing procedure was executed in three distinct stages to ensure uniform dispersion and homogeneity of the constituents. Initially, all dry components were blended for a duration of 5 minutes. This was followed by a wet mixing phase, during which water and the superplasticizer were gradually introduced over approximately 30 minutes to achieve the desired rheological properties. In the final stage, steel fibres were incorporated into the mix, and blending was continued for an additional 10 minutes to ensure even distribution. A schematic representation of the complete mixing sequence is illustrated in Figure 4.

Specimens details

A total of 27 specimens were prepared, combining bar diameter, embedment length, concrete cover, and temperature exposure as detailed in Table 2.

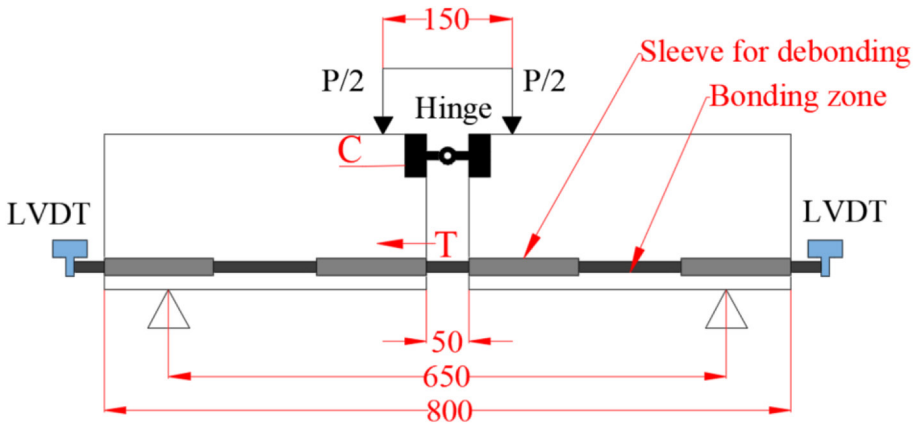

Figure 3. Specimen set up during testing

Table 1. Material proportions of UHPC mix constituents

Material	Quantity	Unit	Weight %
Cement	950	kg	37.06
Silica Fume	190	kg	7.41
Super Plasticizer	39.9	kg	1.56
Fine sand	840	kg	32.77
Quartz powder	210	kg	8.19
Water	176.7	kg	6.89
Steel Fibres	157	kg	6.12
Total weight	2563.6	kg	100%

Reinforcement details

A typical reinforcement for the specimen is illustrated in Figure 5.

Casting and curing specimens

Each specimen was cast under controlled laboratory conditions, with successive layers placed over approximately 10 minutes to minimize the presence of voids. The specimens remained in their moulds for two days prior to demoulding. Subsequently, a steam curing regime was applied for a duration of 28 days to ensure optimal hydration and material performance.

Elevated temperature exposure

Specimens were exposed to 300 °C and 600 °C in a controlled furnace, with controlled heating rates and holding times, then cooled naturally before testing.

Testing apparatus and conditions

All experimental procedures were conducted in the Construction Materials Laboratory at the University of Babylon. Bond tests used a universal testing machine with a load cell and LVDTs to measure load and slip at the steel-concrete interface, Figures 6 and 7. LVDTs and load cell were calibrated. Tests continued until complete specimen failure.

Failure mode identification

The failure mode for each specimen was determined using three complementary methods. First, direct visual observation during testing allowed the identification of physical signs associated with pull-out, partial slip, or steel rupture. Second, continuous video recordings provided a detailed record of the progression of deformation and the exact moment of failure. Third, the load–slip curves were examined to detect characteristic behavioral patterns – such as the onset of slip, sudden drops in load, or non-linear deformation – that distinguish between slip failure, combined failure, and bar rupture. These combined approaches ensured accurate and consistent classification of the failure mechanisms across all tested specimens.

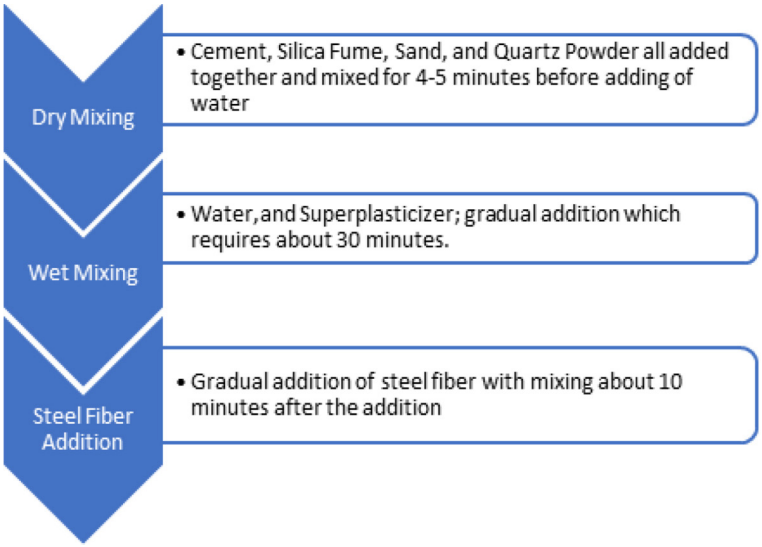

Figure 4. Mixing process

Table 2. Summary of test matrix and specimen coding

Specimen ID	Diameter (mm)	Cover (mm)	Embedment length (mm)	Temp. exposed (°C)
12-1d-6d-RT	12	12	72	RT
12-1d-6d-300	12	12	72	300
12-1d-6d-600	12	12	72	600
12-1d-9d-RT	12	12	108	RT
12-1d-9d-300	12	12	108	300
12-1d-9d-600	12	12	108	600
12-1d-12d-RT	12	12	144	RT
12-1d-12d-300	12	12	144	300
12-1d-12d-600	12	12	144	600
12-2d-6d-RT	12	24	72	RT
12-2d-6d-300	12	24	72	300
12-2d-6d-600	12	24	72	600
12-2d-9d-RT	12	24	108	RT
12-2d-9d-300	12	24	108	300
12-2d-9d-600	12	24	108	600
12-2d-12d-RT	12	24	144	RT
12-2d-12d-300	12	24	144	300
12-2d-12d-600	12	24	144	600
16-1d-6d-RT	16	16	96	RT
16-1d-6d-300	16	16	96	300
16-1d-6d-600	16	16	96	600
16-1d-9d-RT	16	16	144	RT
16-1d-9d-300	16	16	144	300
16-1d-9d-600	16	16	144	600
16-1d-12d-RT	16	16	192	RT
16-1d-12d-300	16	16	192	300
16-1d-12d-600	16	16	192	600

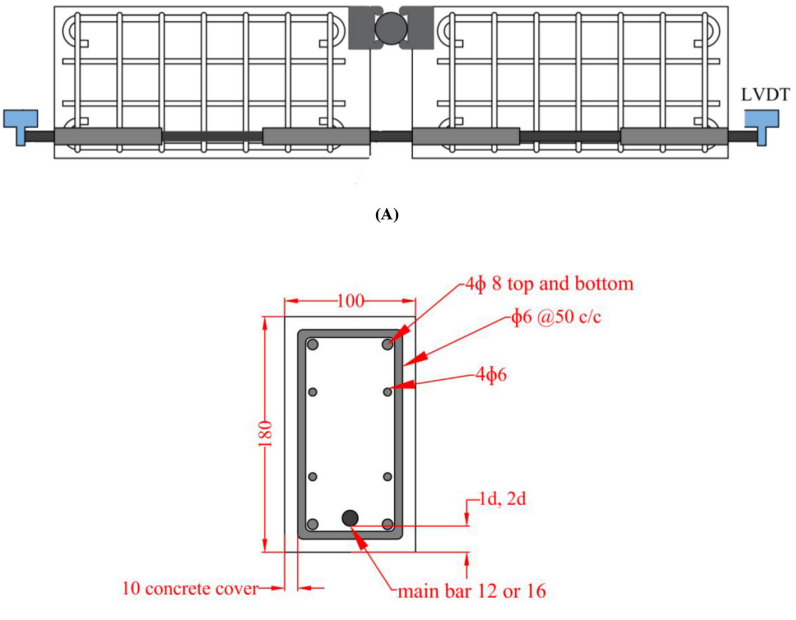

Figure 5. Reinforcing details of the specimen: (A) side view, (B) cross section

Figure 6. Configuration used during specimen testing

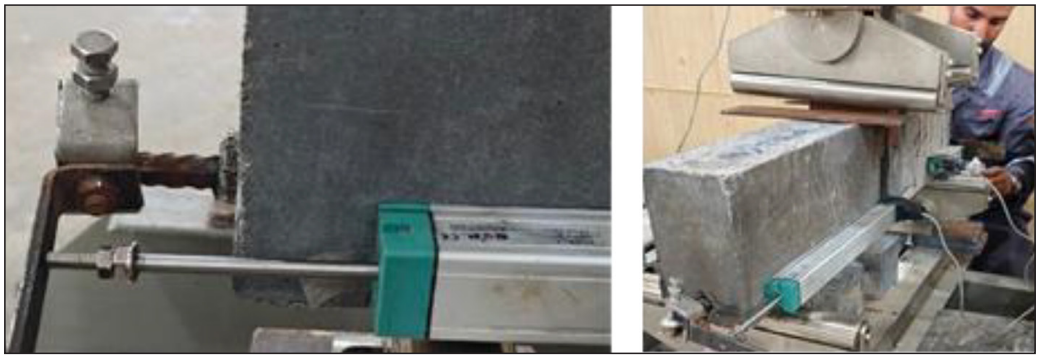

Figure 7. LVDTs installation on both sides

EXPERIMENTAL RESULTS AND INTERPRETATION

High temperature effect

Visual inspection showed minor surface cracks at 300 °C due to water evaporation, but overall matrix integrity remained, Figures 8 and 9. At 600 °C, significant degradation occurred, including microcracking, spalling, discoloration, and increased porosity, indicating substantial loss of mechanical properties, Figure 10.

Presentation of test results

Bond test results are presented as load-slip diagrams, highlighting maximum load capacity and corresponding slip. Full results are illustrated in Table 3.

Beams with '12-1d-6d' and (RT – 300–600 °C)

Figure 11 illustrates the relationship between the applied load and the corresponding slip of the reinforcing steel, recorded up to the point at which a significant reduction in load was observed – an indication of structural failure.

Beams with '12-2d-6d' and (RT – 300–600 °C)

Figure 12 presents the load–slip behaviour of the reinforcing steel in the tested specimens, capturing the response up to the point of failure. Increasing cover to 2d for 6d embedment specimens led to higher capacities. The 300°C specimen achieved 122.7 kN with slip and steel fracture. Room temperature and 600°C specimens failed by pull-out, with 600 °C showing reduced strength (68.5 kN).

Beams with '12-1d-9d' and (RT – 300–600 °C)

Figure 13 illustrates the relationship between the applied load and the slip between the reinforcing steel and the surrounding concrete for the tested specimens. 9d embedment significantly enhanced bond strength. Room temperature showed minimal slip and steel rupture (115.6 kN). The 300 °C specimen reached 130.2 kN with no slip. Even at 600 °C, load was considerably higher (90.6 kN) than 6d embedment, failing by pull-out.

Beams with '12-2d-9d' and (RT – 300–600°C)

Figure 14 illustrates the relationship between the applied load and the corresponding pull (slip)

Figure 8. Free water evaporation

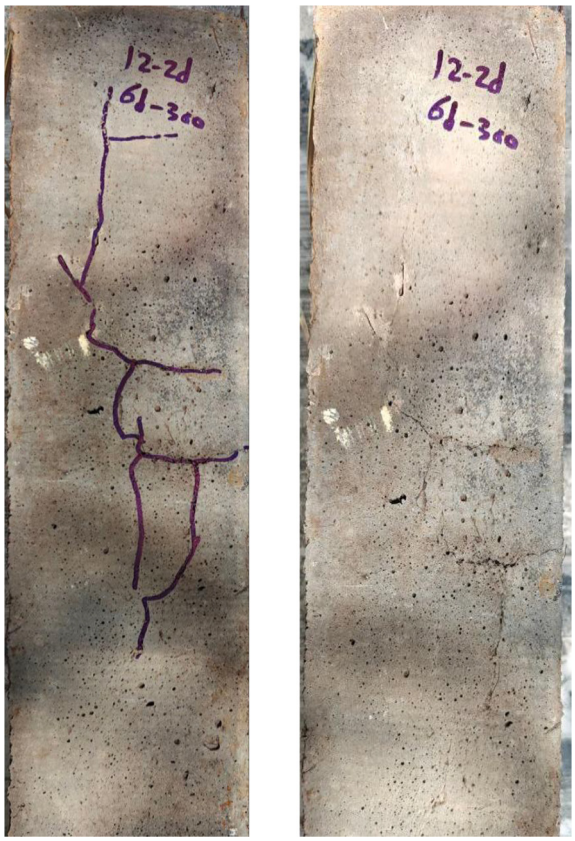

Figure 9. Cracks after exposing to 300 °C

for specimens with an embedment length of 9d and a concrete cover of 2d. For 9d embedment and 2d cover, increased cover further influenced bond, especially at elevated temperatures. The 600 °C specimen showed improved load capacity in comparison with 1d cover.

Beams with '12-1d-12d' and (RT – 300–600 °C)

With 12d embedment, room temperature and 300°C specimens typically failed by steel rupture. Significant load capacities were maintained even at 600°C, Figure 15.

Beams with '12-2d-12d' and (RT – 300–600 °C)

2d cover and 12d embedment generally resulted in highest bond strengths and often led to steel rupture, even at elevated temperatures exhibited near rupture results, Figure 16.

Beams with '16-1d-6d' and (RT – 300–600 °C)

For 16 mm diameter bars, similar trends were observed, with a significant bond strength drop at 600 °C, Figure 17.

Beams with '16-1d-9d' and (RT – 300–600 °C)

Increasing embedment length to 9d for 16mm bars improved bond performance across all temperatures, Figure 18.

Beams with '16-1d-12d' and (RT – 300–600 °C)

With 12d embedment, 16mm bars also showed robust bond behaviour, often leading to steel rupture, Figure 19.

Discussion of key findings

The experimental investigation into the bond behaviour between UHPC and reinforcing steel at elevated temperatures has revealed several important insights with direct implications for structural performance, fire resistance, and design practices. This discussion highlights the most significant findings and interprets their relevance within the context of current knowledge and design needs.

Thermal exposure has a distinct threshold effect

Moderate temperature (300 °C) often maintained or slightly improved bond, possibly due to post-curing [29, 30]. Conversely, 600 °C caused significant bond deterioration,

Figure 10. Spalling after exposing to 600 °C

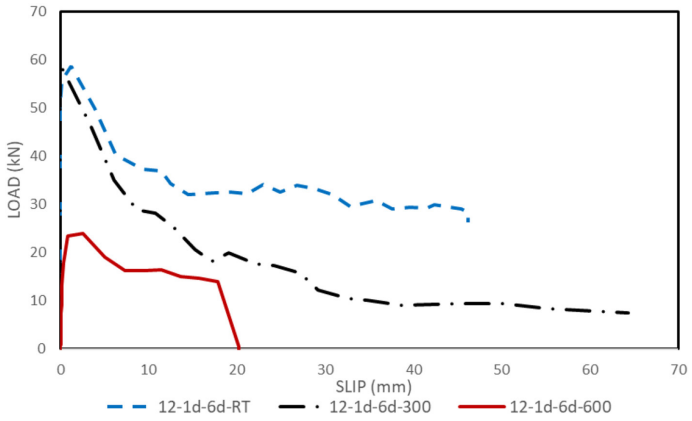

Figure 11. Load – slip diagram for specimens of (12-1d-6d)

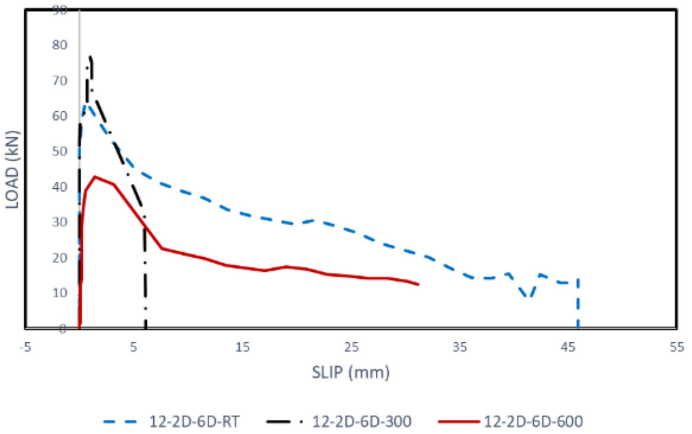

Figure 12. Load – slip diagram for specimens of (12-2d-6d)

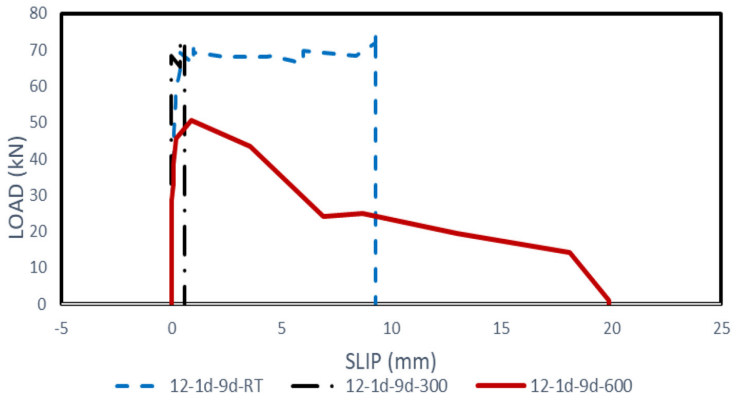

Figure 13. Load – slip diagram for specimens of (12-1d-9d)

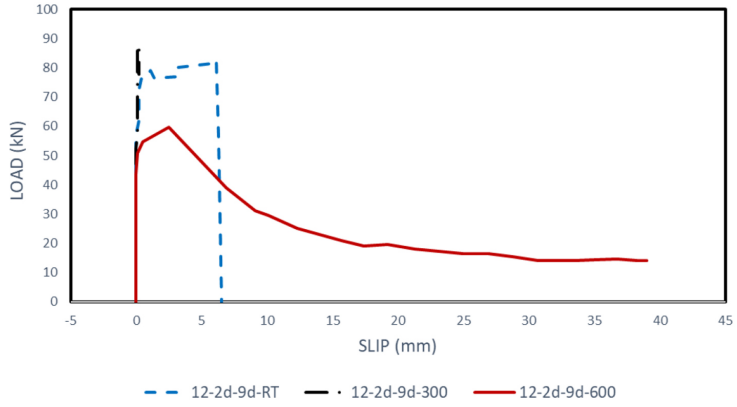

Figure 14. Load – slip diagram for specimens of (12-2d-9d)

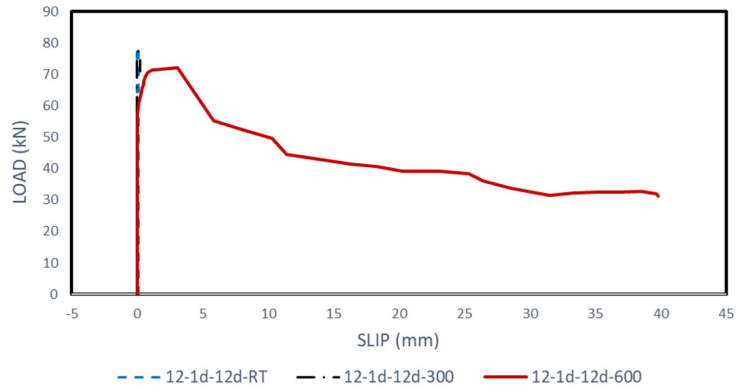

Figure 15. Load – slip diagram for specimens of (12-1d-12d)

indicating it exceeds the UHPC–steel interface's thermal resilience [31]. This is critical for fire-resistant design. At 300 °C, some specimens maintained or even slightly improved their bond strength compared with room temperature because moderate heating can act as a post-curing stage, promoting continued hydration and partial drying of capillary pores without yet causing severe C–S–H or $Ca(OH)_2$ decomposition [32]. This leads to a denser matrix and a stronger interfacial transition zone (ITZ) around the ribs, enhancing adhesion, friction, and mechanical interlock; similar trends of stable or slightly improved mechanical/bond behaviour up to about 300 °C have been reported for high-performance concretes and UHPC by Aslani and Samali [25] (bond at elevated temperature) and in thermal reviews by Zhang et al. (2020) [16], Liang et al. (2022) [33], and Ashteyat et al. (2025) [17].

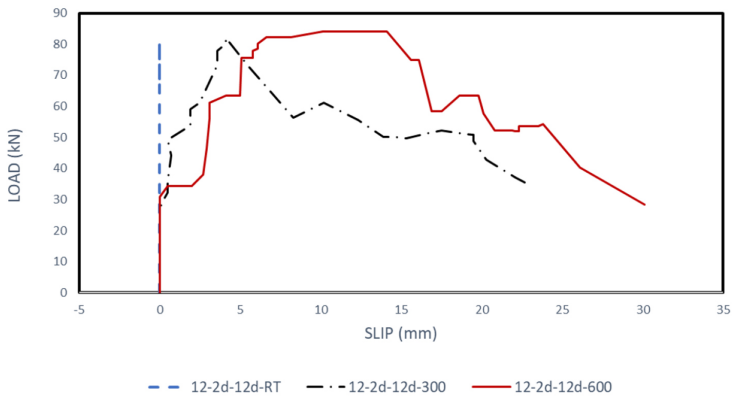

Figure 16. Load – slip diagram for specimens of (12-2d-12d)

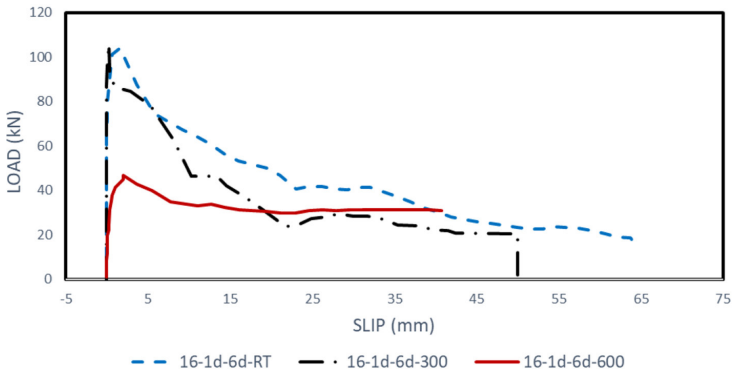

Figure 17. Load – slip diagram for specimens of (16-1d-6d)

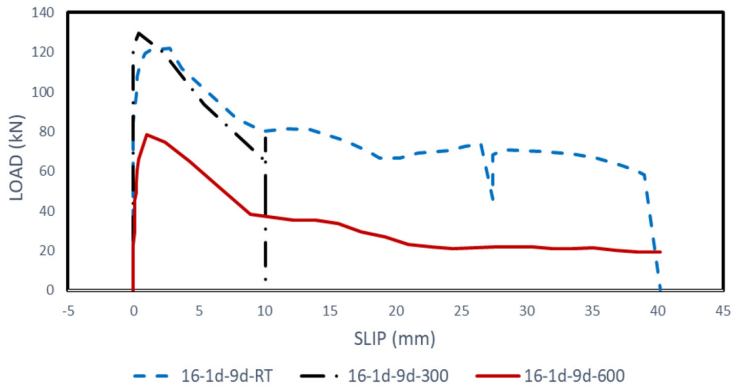

Figure 18. Load – slip diagram for specimens of (16-1d-9d)

At 600 °C, bond loss becomes significant due to severe thermal degradation of the UHPC matrix, including advanced dehydration, C–S–H decomposition, and substantial porosity increase, which reduce the confinement around the bar and promote microcracking and spalling [34]. In addition, differential thermal expansion between steel and UHPC severely damages the ITZ, so that adhesion, friction, and mechanical interlock are strongly diminished, leading to the sharp reduction in bond capacity observed in this study – a behaviour consistent with the critical temperature range (400–600 °C) for bond and matrix breakdown reported by Aslani and Samali (2013) [25] and the UHPC high-temperature reviews of Zhang et al. (2020) [16], Amran et al. (2023) [19], and Ashteyat et al. (2025) [17].

The temperature-dependent trends observed in this study are broadly consistent with recent investigations on UHPC–steel bond under

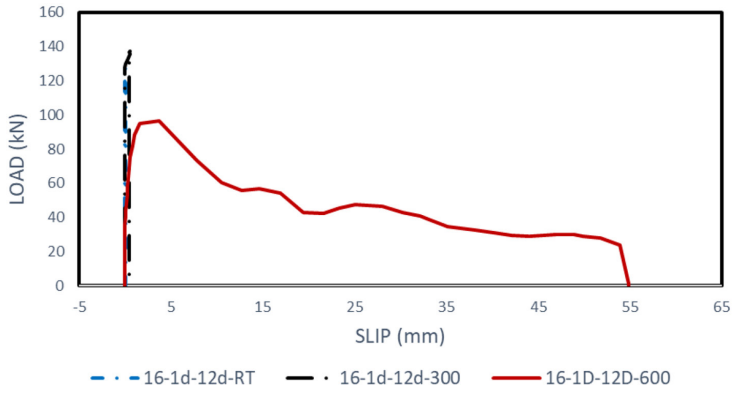

Figure 19. Load – slip diagram for specimens of (16-1d-12d)

Table 3. Summery of the experimental results

ID	Max Load (kN)	Max bond strength (MPa)	Slip (mm)	Failure mode
12-1d-6d-RT	105	38.683	46.2	SLIP
12-1d-6d-300	105.7	38.941	64.3	SLIP
12-1d-6d-600	42.8	15.768	20.2	SLIP
12-1d-9d-RT	102.6	37.799	45.9	SLIP
12-1d-9d-300	122.7	45.204	6.1	COMPINED
12-1d-9d-600	68.5	25.236	31.2	SLIP
12-1d-12d-RT	115.6	28.392	9.3	COMPINED
12-1d-12d-300	130.2	31.978	0.6	STEEL RUPTURE
12-1d-12d-600	90.6	22.252	19.9	SLIP
12-2d-6d-RT	129.6	31.831	6.5	COMPINED
12-2d-6d-300	140.6	34.533	0.2	STEEL RUPTURE
12-2d-6d-600	95.3	23.407	39	SLIP
12-2d-9d-RT	141.2	26.010	0.1	STEEL RUPTURE
12-2d-9d-300	138.8	25.568	0.2	STEEL RUPTURE
12-2d-9d-600	129.1	23.781	39.8	SLIP
12-2d-12d-RT	129.3	23.818	0	STEEL RUPTURE
12-2d-12d-300	131.1	24.150	23	COMPINED
12-2d-12d-600	134.6	24.794	30.1	SLIP
16-1d-6d-RT	176.7	36.618	64	SLIP
16-1d-6d-300	179.6	37.219	50	SLIP
16-1d-6d-600	79.1	16.392	40.2	SLIP
16-1d-9d-RT	206.9	28.584	40.2	SLIP
16-1d-9d-300	219.9	30.380	10.1	COMPINED
16-1d-9d-600	133	18.375	40.2	SLIP
16-1d-12d-RT	215.9	22.371	0.1	STEEL RUPTURE
16-1d-12d-300	234	24.246	0.5	STEEL RUPTURE
16-1d-12d-600	163.8	16.972	54.9	SLIP

elevated temperatures. Pokorný et al. (2020) [30] reported that the bond between prestressing reinforcement and UHPC remained stable or slightly improved at moderate temperatures before degrading significantly at higher levels, which aligns with the present findings of maintained or enhanced bond performance at 300 °C and marked deterioration at 600 °C. Similarly, Tang et al. (2022) [29] showed that high-temperature exposure modifies the local bond–slip response

between UHPC and reinforcing bars, leading to reduced bond strength and increased slip, comparable to the larger slips and shift to pull-out failure observed here at 600 °C.

Embedment length is the most influential mechanical parameter

Longer embedment lengths consistently enhanced bond strength, distributing stress and often leading to steel rupture. At 600 °C, 12d embedment still showed high performance, emphasizing its necessity in fire-exposed environments. Increasing the embedment length from 6d to 9d and 12d generally enhanced bond performance by providing a larger surface area for stress transfer, delaying slip, and often shifting the failure mode from pull-out at 6d to combined failure or steel rupture at 9d–12d, especially at room temperature and 300 °C. This behaviour is evident in specimens such as 12-1d-6d versus 12-1d-9d and 12-1d-12d, and in 16-1d-6d versus 16-1d-9d and 16-1d-12d, where longer embedment lengths developed higher bar forces and much smaller slips, indicating a more fully developed bond.

However, the increase in "average bond stress" with embedment length is not proportional and can even appear to reduce at longer lengths, because the average bond stress is calculated by dividing the maximum bar force by the product of bar perimeter and embedment length. Once the bond becomes strong enough for the bar to approach yielding or rupture, the steel capacity rather than the bond controls the maximum load, so further increases in embedment mainly redistribute bond stress and change the failure mode, rather than producing a linear gain in average bond stress.

Steel rupture in specimens such as 12-1d-12d-300, 12-2d-6d-300, 12-2d-9d-RT/300 and 16-1d-12d-RT/300 occurred because the UHPC–steel bond capacity exceeded the tensile capacity of the reinforcing bars, so the failure mode changed from bond-controlled to steel-controlled. This is mainly due to the combination of a dense, high-strength UHPC matrix, long embedment lengths (9d–12d) that mobilise a large bond surface, and adequate cover (especially 2d) that prevents premature splitting and maintains confinement, allowing full stress transfer into the bar.

Microstructurally, the strong ITZ in UHPC limits slip and microcracking around the ribs, so adhesion, friction and mechanical interlock develop almost fully until the bar yields and finally ruptures. Similar behaviour – steel rupture instead of bond failure when bond strength in high-strength or UHPC systems exceeds bar capacity – has been reported in ACI 408R-03 [35] and in bond studies on high-performance concretes at elevated temperatures by Aslani and Samali [25] and Xu et al [23].

Concrete cover enhances bond strength but has diminishing returns at high temperature

Increased concrete cover improved confinement at room temperature and 300 °C [36]. However, its effect was less pronounced at 600 °C, suggesting its protective role diminishes as the UHPC matrix degrades. Design should pair optimized embedment with adequate cover.

Effect of bar diameter on bond behaviour

In this experimental program, increasing the bar diameter from 12 mm to 16 mm generally led to higher maximum bar forces but slightly lower average bond stresses, because the larger bars develop greater tensile forces while the bond capacity per unit surface does not increase proportionally. This trend is visible in the summarized results, where 16 mm bars (e.g. 16-1d-6d-RT/300) carry higher loads than 12 mm bars with the same embedment length, yet the calculated bond stress (load divided by perimeter × length) is of similar magnitude or marginally lower, especially after exposure to elevated temperatures.

Mechanically, larger bars require more bond force to anchor the higher steel stresses, and the surrounding concrete must provide greater confinement to prevent splitting and pull-out, so any thermal damage or microcracking in UHPC has a more pronounced effect on the effective bond stress of 16 mm bars. Similar observations have been reported in the literature on bond at elevated temperatures, where increasing rebar diameter tends to reduce bond strength per unit area and steepen the post-peak bond–slip response, as highlighted in analytical models by Aslani and Samali (2013) [25] and in recent experimental studies on bar diameter effects in post-fire and elevated-temperature bond behaviour

In terms of bond and slip, the 16 mm bars generally exhibited larger slip at failure than the 12 mm bars under comparable embedment and temperature, particularly at 600 °C, showing that once thermal cracking reduces confinement,

larger diameters are more prone to progressive pull-out and greater interface deformation even when their average bond stress per unit surface is similar or slightly lower.

Deviations highlight complex interactions

Minor inconsistencies underscore the complex, multi-parameter nature of bond behaviour. Holistic design considering cover, embedment, bar diameter, and thermal conditions is essential.

Slip values varied notably between specimens, even for similar bar diameters and embedment lengths, because bond behaviour in UHPC is highly sensitive to the governing failure mode and the local cracking and confinement around the bar, especially after thermal exposure. Specimens with lower bond capacity (e.g. short embedment or degraded matrix at 600 °C) failed by pure slip (pull-out), where progressive debonding at the UHPC–steel interface allowed large bar displacement before failure, whereas specimens with stronger bond (long embedment, higher cover, or steel-rupture/combined failure) mobilised strong adhesion, friction, and mechanical interlock, reached high bar stresses with minimal pull-out, and thus exhibited very small slip values. Consequently, the scatter in slip mainly reflects differences in bond capacity and failure mode (pull-out versus steel-controlled failure) rather than variability in material quality.

Implications for practice and design

Specimens that exhibited zero or nearly zero slip at failure correspond to cases where the governing failure mode was steel-controlled rather than bond-controlled. In these specimens, the UHPC–steel bond was sufficiently strong to prevent noticeable pull-out, so that the reinforcing bar reached yielding and rupture with only negligible relative displacement at the interface. This behaviour is associated with configurations providing high confinement and a large, bonded surface, particularly those combining long embedment lengths (9d–12d) with increased concrete cover (2d), which enhance adhesion, friction and mechanical interlock along the bar. Consequently, the very small, recorded slip values in such cases reflect a dominant steel-rupture failure mode within a well-confined UHPC matrix, where bond capacity exceeds the tensile capacity of the reinforcement.

Findings emphasize specifying appropriate embedment lengths for thermal conditions, recognizing the limited protective role of cover alone under severe fire, and designing reinforcement details for bond degradation. Leveraging UHPC's thermal resilience, with caution beyond 300 °C, is also important. This study contributes to a nuanced understanding of UHPC bond behaviour in fire/high-temperature scenarios, supporting reliable design recommendations.

CONCLUSIONS

The experimental findings highlighted several key factors influencing the bond behaviour between UHPC and reinforcing steel under elevated temperatures. Temperature emerged as a critical variable; while exposure to 300 °C sometimes preserved or marginally enhanced bond strength, a significant reduction was observed at 600 °C, where most specimens failed through slippage or pull-out, indicating a loss of effective bond beyond this thermal threshold. Embedment length proved to be the most influential parameter – extending embedment from 6d to 12d consistently improved bond performance, reduced slippage, and shifted failure modes from bond-related failures to steel rupture, even at elevated temperatures. Concrete cover also contributed to enhanced bond strength, particularly under ambient and moderate thermal exposure, by delaying crack initiation and slippage. However, its effect diminished at higher temperatures, especially when adequate embedment was already present. Failure modes were observed to evolve with both temperature and specimen geometry: steel rupture was predominant at room temperature, mixed failure mechanisms became common at 300 °C, and pull-out failures were dominant at 600 °C, reflecting the progressive deterioration of bond integrity under thermal stress. Additionally, the results suggested complex interactions among variables, as some specimens with thinner covers still performed effectively due to sufficient embedment, while other anomalies were likely influenced by local effects such as microcracking or surface spalling.

Based on the overall comparison of all parameters, the specimens that demonstrated the highest bond performance were those combining a 12 mm bar diameter with the longest embedment length (12d) and the largest concrete cover (2d), particularly at room temperature and 300 °C. These configurations consistently

developed the highest bond stresses and exhibited steel-rupture failure modes, indicating that the UHPC-steel bond capacity exceeded the tensile capacity of the reinforcement. In contrast, elevated temperatures of 600 °C significantly reduced bond performance across all parameter combinations. Accordingly, the optimal bond behaviour in this study is achieved with the combination (12 mm bar – 12d embedment – 2d cover – RT/300 °C).

Acknowledgments

The author would like to express his sincere gratitude to Dr. Majid M. A. Kadhim, the supervisor of the master's thesis and the second author of this manuscript, for his invaluable guidance, continuous support, and insightful supervision throughout the preparation of this research. His expertise and dedication played a fundamental role in the successful completion of this study.

REFERENCES

1. Yıldırım G, Şahmaran M, Anıl Ö. Engineered cementitious composites-based concrete. Eco-efficient repair and rehabilitation of concrete infrastructures. 2018:387–427.
2. Zaid O, Al-Ezzi MJ, Al-Dala'ien RN, Ahmed M, Anas SM. State of the art review on ultra-high-performance fiber reinforced concrete properties standardization and structural applications. Discover Sustainability. 2025;7(1):83.
3. Du J, Meng W, Khayat KH, Bao Y, Guo P, Lyu Z, et al. New development of ultra-high-performance concrete (UHPC). Composites Part B: Engineering. 2021;224:109220.
4. Surendran H, Akhas PK. Properties of high-performance concrete incorporating toughened glass waste coarse aggregate: An experimental study. Structures. 2024;60:105897.
5. Aïtcin PC. The durability characteristics of high performance concrete: A review. Cement and Concrete Composites. 2003;25:409–20.
6. Gutierrez PA, Cánovas MF. High-performance concrete: requirements for constituent materials and mix proportioning. Materials Journal. 1996;93(3):233–41.
7. Fehling E, Schmidt M, Walraven J, Leutbecher T, Fröhlich S. Ultra-high performance concrete UHPC. Ernst & Sohn: Berlin, Germany. 2014.
8. Lantsoght EO, van der Veen, C., De Boer, A., van der Ham H. Long-term material and structural behavior of high-strength concrete cantilever bridge: Results of 20 years monitoring. Structural concrete. 2018;19(5):1079–91.
9. ACI. Ultra-High-Performance Concrete: An Emerging Technology Report. 2018. Contract No.: 48331.
10. Akhnoukh AK, Buckhalter C. Ultra-high-performance concrete: Constituents, mechanical properties, applications and current challenges. Case Studies in Construction Materials. 2021;15:e00559.
11. Shafieifar M, Farzad M, Azizinamini A. Experimental and numerical study on mechanical properties of Ultra High Performance Concrete (UHPC). Construction and Building Materials. 2017;156:402–11.
12. Shunmuga Vembu PR, Ammasi AK. A comprehensive review on the factors affecting bond strength in concrete. Buildings. 2023;13(3):577.
13. Khalifa M, Youssef MA, Alhadid MMA. Heat of hydration stresses in stainless-steel-reinforced-concrete sections. Sustainability. 2020;12(12):4852.
14. Yang Y, Ismail M, Pantazopoulou S, Palermo D. Tensile behaviour of ultra-high-performance steel fiber reinforced concrete. Canadian Journal of Civil Engineering. 2021;48(11):1409–21.
15. Bolina FL, Poleto G, Christ R. Thermal parameters of UHPC in case of fire: an approach to the Brazilian standard ABNT NBR 15200. Revista IBRACON de Estruturas e Materiais. 2024;17:e17508.
16. Zhang P, Kang L, Wang J, Guo J, Hu S, Ling Y. Mechanical properties and explosive spalling behavior of steel-fiber-reinforced concrete exposed to high temperature – a review. Applied Sciences. 2020;10(7):2324.
17. Ashteyat A, Shhabat M, Alkhalaileh A, Al-Zu'bi M, Abdel-Jaber Mt. Behavior of ultra-high-performance concrete under elevated temperatures: A comprehensive review of mechanical, physical, thermal, and microstructural properties. Results in Engineering. 2025;26:104960.
18. Liang X, Wu C, Su Y, Chen Z, Li Z. Development of ultra-high performance concrete with high fire resistance. Construction and Building Materials. 2018;179:400–12.
19. Amran M, Murali G, Makul N, Kurpińska M, Nehdi ML. Fire-induced spalling of ultra-high performance concrete: A systematic critical review. Construction and Building Materials. 2023;373:130869.
20. Committee A. Bond and development of straight reinforcing bars in tension. ACI 408R-03), American Concrete Institute, Farmington Hills, Mich. 2003;48.
21. Mindess S, Young F, Darwin D. Concrete 2nd editio. Technical Documents. 2003;585.
22. Yogendran V, Langan B, Haque M, Ward M. Silica fume in high-strength concrete. Materials Journal. 1987;84(2):124–9.

23. Xu Q, Jiang X, Lv H, Xu C. Experimental investigation on bond-slip performance and damage evolution mechanism of deformed reinforcing bar embedded in steel polyvinyl-alcohol hybrid fiber high performance concrete after high temperature. Construction and Building Materials. 2024;436:136951.
24. Algourdin N, Pliya P, Beaucour AL, Simon A, Noumowé A. Influence of polypropylene and steel fibres on thermal spalling and physical-mechanical properties of concrete under different heating rates. Construction and Building Materials. 2020;259:119690.
25. Aslani F, Samali B. Predicting the bond between concrete and reinforcing steel at elevated temperatures. Structural engineering & mechanics. 2013;48:643–60.
26. Nadir Y, A S. Bond strength determination between coconut shell aggregate concrete and steel reinforcement by pull out test. Asian Journal of Civil Engineering. 2018;19.
27. Rilem T. RILEM recommendations for the testing and use of constructions materials. RC. 1994;6:218-20.
28. CEN. Steel for the reinforcement of concrete: Weldable reinforcing steel – General. EN 10080. 2005.
29. Tang C-W. Effect of high temperatures on local bond-slip behavior between rebars and UHPC. Struct Eng Mech. 2022;81(2):163–78.
30. Pokorný P, Kolísko J, Čítek D, Kostelecká M. Effect of elevated temperature on the bond strength of prestressing reinforcement in UHPC. Materials. 2020;13(21):4990.
31. Wang R, Ma B, Chen X. Experimental study on bond performance between UHPC and steel bars. Journal of Building Engineering. 2023;79:107861.
32. Farage M, Sercombe J, Gallé C. Rehydration and microstructure of cement paste after heating at temperatures up to 300 °C. Cement and Concrete Research. 2003;33:1047–56.
33. Liang R, Huang Y, Xu Z. Experimental and analytical investigation of bond behavior of deformed steel bar and ultra-high performance concrete. Buildings. 2022;12(4):460.
34. Kodur V, Banerji S, Solhmirzaei R. Effect of temperature on thermal properties of ultrahigh-performance concrete. Journal of Materials in Civil Engineering. 2020;32:04020210.
35. Allen JH, Felder AL, McDermott JF, Azizinamini A, Frosch RJ, Mitchell D, et al. Bond and development of straight reinforcing bars in tension. American Concrete Institute, Detroit, MI, USA, Rep ACI 408R-03. 2003.
36. Cuong NH, Luat N-V, Nguyen M-ST, Lee DH, Yoo YJ, Lee K. Effect of concrete cover and embedment length on bond strength of steel reinforcement in UHPC: An experimental and numerical approach. Case Studies in Construction Materials. 2025;23:e05504.